A detailed quartz and feldspar luminescence chronology for the Khonako II loess section (South Tajikistan)

Amelie Challier, Kristina J Thomsen, Redzhep Kurbanov, Piotr Sosin, Andrew Murray, Guillaume Guérin, Olga Meshcheryakova, Asliddin Karayev, Farhad Khormali, Natalia Taratunina, et al.

Journal Pre-proof

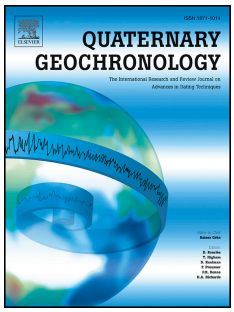

A detailed quartz and feldspar luminescence chronology for the Khonako II loess section (South Tajikistan)

Amelie Challier, Kristina J. Thomsen, Redzhep Kurbanov, Piotr Sosin, Andrew Murray, Guillaume Guerin, Olga Meshcheryakova, Asliddin Karayev, Farhad Khormali, Natalia Taratunina, Anna Utkina, Jan-Pieter Buylaert

PII: S1871-1014(24)00075-X

DOI: https://doi.org/10.1016/j.quageo.2024.101571

Reference: QUAGEO 101571

To appear in: *Quaternary Geochronology*

Received Date: 14 November 2023

Revised Date: 19 April 2024

Accepted Date: 10 June 2024

Please cite this article as: Challier, A., Thomsen, K.J., Kurbanov, R., Sosin, P., Murray, A., Guerin, G., Meshcheryakova, O., Karayev, A., Khormali, F., Taratunina, N., Utkina, A., Buylaert, J.-P., A detailed quartz and feldspar luminescence chronology for the Khonako II loess section (South Tajikistan), *Quaternary Geochronology*, https://doi.org/10.1016/j.quageo.2024.101571.

A detailed quartz and feldspar luminescence chronology for the Khonako II loess section (South Tajikistan)

Amélie Challier[1, *], Kristina J. Thomsen[1], Redzhep Kurbanov[2], Piotr Sosin[2], Andrew Murray[3], Guillaume Guérin[4], Olga Meshcheryakova[5], Asliddin Karayev[6], Farhad Khormali[7], Natalia Taratunina[1], Anna Utkina[8], Jan-Pieter Buylaert[1]

[1]Department of Physics, Technical University of Denmark, DTU Risø Campus, 4000 Roskilde, Denmark

[2]Institute of Water Problems, Hydropower and Ecology, National Academy of Sciences of Tajikistan, 734063 Dushanbe, Republic of Tajikistan

[3]Nordic Laboratory for Luminescence Dating, Department of Geoscience, Aarhus University, and DTU Physics, DTU Risø Campus, 4000 Roskilde, Denmark

[4]Université de Rennes, CNRS, Géosciences Rennes, UMR 6118, 35000 Rennes, France

[5]School of Geography and Ocean Sciences, Nanjing University, Nanjing, China

[6]Institute of History, Archaeology and Ethnography, NAST, 734063 Dushanbe, Republic of Tajikistan

[7]Gorgan University of Agricultural Sciences and Natural Resources, Department of Soil Sciences, Gorgān, Iran

[8]Research Center for Geochronology and Isotope analysis, Korea Basic Science Institute, Chungbuk 28119, South Korea

*Corresponding author: ajmch@dtu.dk

Abstract

Parts of Central Asia have been dominated by high dust flux since the start of the Quaternary. The resulting loess-palaeosol deposits are important archives for landscape and climate changes, but there is a lack of chronological data for the subaerial deposits of Southern Tajikistan. Our study presents a high-resolution luminescence chronology for the Khonako II section in the Khovaling region. Thirty-seven samples were collected from the first ~ 8 m of the section, corresponding to the Holocene soil and the upper part of the Loess 1 (L1) unit. We applied quartz OSL dating to the coarse silt fraction (40-63 µm) and polymineral $pIRIR_{200,290}$ dating to the very fine sand fraction (63-90 µm). The polymineral $pIRIR_{200,290}$

signal has satisfactory characteristics. The quartz dose response curve displays a non-single exponential growth above ~ 100 Gy, thus, the D_e values were estimated by fitting a single exponential function plus linear component to the dose response data. To assess the $pIRIR_{200,290}$ residual dose at deposition, we used the offset between our quartz and polymineral chronologies from Khonako II and equivalent doses measured on modern dust samples from Tajikistan and Uzbekistan. The resulting 9.2±0.4 Gy dose was then subtracted from the $pIRIR_{200,290}$ doses for final age calculation. The quartz OSL and pIRIR ages are then generally consistent. The obtained high-resolution luminescence chronology shows that the upper part of the L1 unit accumulated during the end of marine isotope stage (MIS) 3 and through MIS 2 (39 to 20 ka). The average dust accumulation rates (DARs) increased from ~31 cm ka^{-1} to 41 cm ka^{-1} between MIS 3 and MIS 2. The DAR reached a peak of ~71 cm ka^{-1} at 21 ka. A hiatus of ~7-9 ka was then identified between the end of the last glacial maximum (LGM) and the beginning of the Holocene, and the average DAR decreased during the Holocene. Our results indicate a continuous high dust flux in the Khovaling plateau over the last 39 ka, but reworking processes and potential deflation events mark the LGM-Holocene transition. High-resolution luminescence dating studies in Tajikistan are therefore important to detect potential discontinuities in the sequences and provide an independent timescale for interpreting the climate proxies and calculating dust accumulation rates.

Keywords: Southern Tajikistan, quartz OSL dating, polymineral $pIRIR_{200,290}$ dating, high-resolution dating, dust accumulation rates

1. Introduction

Loess deposits in Central Asia are well-known for providing exceptional palaeoclimate and palaeoenvironmental archives. In the last ~2.7 Ma, dust from deflation processes under arid and semi-arid conditions has been transported by westerly winds and is believed to be deposited almost continuously (Zan et al., 2022). Most of the thickest loess sections are located on the mountain footslopes of the Pamirs in the Afghan-Tajik depression (Southern Tajikistan), with up to ~200 m of accumulated sediment. These loess deposits consist of alternating thick loess units (L), resulting from high dust accumulation rates during glacial periods, and palaeosols forming pedocomplexes (PCs) developed during interglacial periods under warmer and wetter climatic conditions. This alternating formation of loess and palaeosol units records climate stages and landscape evolution during the Quaternary (Ding et al., 2002; Li et al., 2020).

Loess-palaeosol sequences in the Afghan-Tajik depression are characterised by a considerable thickness, reaching 200 m in several outcrops, a large number of well-defined palaeosols, forming up to 40 PC's in the most complete sections, and a semi-continuous chronology, covering the entire Quaternary. This makes the loess-palaeosol sequences of Southern Tajikistan an important archive of Central Asian climate and landscape history. The most complete loess-palaeosol sections have been described in the Khovaling loess plateau in the piedmonts of the Pamirs (Dodonov, 2002; Ding et al, 2002; Dodonov and Zhou, 2008). The current chronology of the Tajik loess sections is based mainly on magnetostratigraphy and frequency-dependent magnetic susceptibility (Dodonov, 1991; Dodonov and Zhou, 2008; Parviz et al., 2020; Zan et al., 2022), and numerous studies have suggested that the Central Asian loess chronostratigraphy can be correlated with the Chinese Loess Plateau (CLP) and $\delta^{18}O$ records (Dodonov and Baiguzina, 1995; Ding et al., 2002; Dodonov et al., 2006; Dodonov and Zhou, 2008; Parviz et al., 2020; Tian et al., 2021). However, this assumption relies on the continuity and integrity of the sedimentary record, an assumption not yet tested for the subaerial deposits of Southern Tajikistan, which could be affected by erosion and slope post-depositional processes.

Determining high-resolution numerical chronologies for the Southern Tajik loess sequences is important to ensure an independent timescale for interpreting climate proxies, such as grain size and magnetic susceptibility, and accurate correlation of the palaeosols with the global climate. High-resolution luminescence dating studies can also reveal discontinuities in the sedimentary record. Frechen and Dodonov (1998) were the first to apply luminescence dating to Tajik loess, and they coupled high-resolution (n=74) thermoluminescence (TL) and infrared stimulated luminescence (IRSL) with an IR stimulation at 50°C (IR_{50}) dating in the Darai Kalon section down to the Bruhnes/Matuyama boundary between PC9 and PC10. They obtained a good agreement between their TL and fading uncorrected IRSL ages up to PC1 (~80 ka), confirming the correlation suggested from the palaeomagnetic record between PC1 and the last interglacial soil layer (S1) of the CLP record. Below PC1, the IRSL dose underestimation and the scatter between the ages prevented the establishment of a reliable chronology (Frechen and Dodonov, 1998).

The IR_{50} signal is known to suffer from anomalous fading (e.g. Spooner, 1994) which usually results in an underestimation of the true burial age. Since the recent methodological developments in luminescence dating in terms of measurement procedure (single-aliquot regenerative-dose [SAR] protocol, Murray and Wintle, 2000) and the discovery of a more stable feldspar signal (post-IR IRSL [pIRIR], Thomsen et al, 2008; Thiel et al., 2011; Li and Li, 2011;), most studies in loess are now based on quartz SAR optically stimulated luminescence (OSL) (e.g., Buylaert et al., 2007, 2008; Lai et al., 2010) and/or K-rich feldspar

SAR post-IR IRSL ages (e.g., Buylaert et al., 2012, 2015; Li and Li, 2012a; Li et al., 2015, Yi et al., 2016, 2018; Stevens et al., 2018; Zhang et al., 2023). Because of the high dose rates in loess (~ 3 Gy ka^{-1}), the OSL signal from quartz can only be used to date the last ~50 ka, whereas feldspar has the potential to extend the chronological range to ~250 ka (Buylaert et al., 2007; Li and Li, 2011).

In southern Central Asia, quartz OSL dating has been applied to obtain a numerical chronology from the Holocene to the last glacial period on several loess sections in Southern Tajikistan and the Tajik Basin (Wang et al., 2018; Yang et al., 2020; Song et al., 2021; Tian et al., 2021). Luminescence sensitivity studies have also been carried out on the Karamaidan loess section from MIS 9 to MIS 19 (Dave et al., 2022) and the Khonako III section from L1 to PC2 (Li and Zhou, 2021). These authors highlighted an increase in sensitivity of the quartz signal in the pedocomplexes units that might be linked to either a change in source or to repeated irradiation and bleaching cycles during transportation processes. However, no chronology was presented for the Khonako III section. Thus, luminescence chronologies are limited for the Southern Tajik loess record, and the application of pIRIR protocols has not yet been tested in this area. Li et al. (2020) successfully applied a $pIRIR_{200,290}$ protocol to loess sections in the northern margins of the Tianshan Mountains, China. These authors considered their feldspar ages reliable up to ~250 ka, but that the quartz OSL ages start to underestimate the feldspar ages beyond ~40 ka. These results highlight the potential of the method for Central Asian loess-palaeosol sequences.

This study presents a detailed luminescence chronology for the Holocene soil and the upper part of the L1 unit of the Khonako II section in Southern Tajikistan. We test the applicability of quartz OSL and polymineral $pIRIR_{200,290}$ measurement protocols and compare the offset between the resulting ages with those estimated on modern dust samples to assess the residual dose at deposition of the $pIRIR_{200,290}$ signal.

2. Site description and sampling

The Khonako site (N 38.35959° E 70.04552°) is located in the Tajik-Afghan depression (Southern Tajikistan), about 10 km northeast of Khovaling (Fig. 1). As a result of a series of landslides, three cirques have formed at this location: the western (geological section Khonako-II), which is 1 km long and opens up to 16-18 PC's, central (palaeolithic site Khonako-III), ~350 m long, and eastern (geological section Khonako-I), about 300 m long, all separated by small promontories. The Khonako III outcrop is well-known for its archaeological finds with Middle Palaeolithic industries in PC1 and PC2 and artefacts from the Lower Palaeolithic in PC3 and PC4 (Schäfer et al., 1998). The Khonako II section (altitude 1890 m) is considered to be one of the best-preserved loess sections in the Khovaling

Plateau; up to 16 PCs have been identified, providing a sedimentary record presumably back to ~MIS 31 (Dodonov, 2002). The Holocene cover in loess areas of Tajikistan is heavily eroded due to modern agriculture (Murray et al, to be submitted) and is present in only a few locations in the Khovaling plateau. The Holocene soil at Khonako II is 2 m thick and is the thickest preserved Holocene section among the loess records of the Khovaling region. The L1 unit is developed over 12.2 m. We excavated the top part of the Khonako-II outcrop in 2019; two geological trenches were dug in the middle part of the outcrop and opened up 40.8 m of in-situ sediments to the top of L3. The trenches were divided into forty-three sections of between 0.5 and 1.5 m length. A field description of the loess and palaeosol layers was made and samples for magnetic susceptibility measurements and sedimentological analyses collected. Metal or plastic sampling tubes for luminescence dating were hammered into the surface cleaned sections every ~10 to 30 cm.

In addition, modern dust samples were collected in 2022 and 2023 after mild dust storms, which occur regularly in Tajikistan in summer and autumn. Dust was scraped off various surfaces in areas remote from construction work. Our samples include only dust of natural origin and long-distance transport material. The first sample was collected near Termez city (Uzbekistan), 150 km southwest of Khovaling; the second and third samples were collected near Dushanbe and Gissar cities (100 km northwest of Khovaling).

In this study, thirty-seven samples are used to develop a luminescence chronology for the top 8 metres, corresponding to the Holocene soil and upper part of the L1 unit (Figs. 1c,2, Table S1).

Fig. 1.

3. Materials and methods

3.1. Sample preparation

The samples were prepared under dim orange light (Sohbati et al., 2021) using standard procedures (e.g. Murray et al., 2021). The outer five cm of each tube end were removed and used for high-resolution gamma spectrometry measurements. Because of the relatively high carbonate content of the sediment, a first 10 % HCl treatment was applied before wet sieving, and the 63-90 and 40-63 µm fractions were kept for further analyses. To ensure the removal of carbonates, a second 10 % HCl treatment was then applied, followed by a 10% H_2O_2 treatment to remove organic matter. Because of the fine-grained nature of the sediment and thus limited fractions, heavy liquid separation was not carried out and $pIRIR_{200,290}$ measurements were performed on the polymineral 63-90 µm fraction. The coarse-silt quartz

fraction (40-63 µm) was treated with 35% H_2SiF_6 for three to four days to remove the feldspar grains.

3.2. Luminescence measurements

All measurements were made using Risø TL/OSL readers equipped with calibrated $^{90}Sr/^{90}Y$ beta sources (Bøtter-Jensen et al., 2010; Hansen et al., 2018; Autzen et al., 2022). Polymineral samples were optically stimulated using 870 nm IR LEDs (between 135 and 350 mW cm^{-2}), and the IRSL signal was detected using a blue filter combination (4 mm of Corning 7–59 in combination with 2 mm Schott BG 39). Quartz stimulation was achieved using 470 nm blue LEDs (between 40 and 100 mW cm^{-2}), and the OSL signal was detected through a 7.5 mm Hoya U-340 filter.

We used a $pIRIR_{200,290}$ SAR protocol (Li and Li, 2012b; Buylaert et al., 2012, 2015; Yi et al., 2015; Stevens et al., 2018) with a preheat of 320 °C for 60 s to measure the polymineral samples (Ø=2 mm for aliquots, hundreds of grains per aliquot). The first infrared stimulation was carried out at 200 °C for 200 s, followed by a second IR stimulation at 290 °C of the same duration. The size of the test dose was equivalent to ~100% of the expected dose. At the end of each SAR cycle, the polymineral aliquots were bleached using an elevated-temperature IR stimulation (325 °C for 200 s). The first 2 s of the $pIRIR_{290}$ signal was used for dose estimation. The last 40 s was used to estimate background.

The coarse-silt quartz samples were measured as multi-grain aliquots (Ø=2 or 8 mm for aliquots, hundreds to thousands of grains per aliquot) using a standard SAR quartz protocol (Murray and Wintle, 2000, 2003) with a preheat of 240 °C (10 s), a cutheat of 200 °C, and a high-temperature bleach at 280 °C for 100 s between SAR cycles to minimise potential recuperation (Murray and Wintle, 2003). The quartz OSL signals were measured using the blue LEDs at 125 °C for 40 s. In the analysis, we summed the initial 0.48 s of stimulation and estimated the background from the subsequent 0.64 s (early background subtraction; Ballarini et al., 2007; Cunningham and Wallinga, 2010).

The quartz purity was assessed using an OSL IR depletion ratio test (Duller, 2003). Seven samples (228850, 228856, 228860, 228861, 228862, 228864, 228866) displayed unsatisfactory average OSL IR depletion ratios (average of 0.82±0.04) and were subsequently discarded from the OSL dataset. For the accepted samples, a comparison between the average sensitivity corrected OSL IR depletion ratio (0.970±0.010) and the blue-stimulated recycling ratio (0.971±0.007, n = 156, 30 samples) confirms the absence of a significant IRSL signal and the ability of the protocol to adequately correct for sensitivity changes.

3.3. Dose rates

Given the fine-grained nature of the sediment and the risk of losing the feldspar grains during the etching process, we decided not to etch our very fine sand fraction (63-90 µm) and instead take the alpha component into account. We use an a-value of 0.09±0.02 (Schmidt et al., 2018) and an alpha attenuation factor of 0.30±0.05 (Martin et al., 2014). External beta dose rate attenuation factor was calculated following Mejdahl (1979). The internal beta dose rate contribution is based on an assumed 12.5±0.5 % K content (Huntley and Baril, 1997). For the quartz (40-63 µm) alpha component, we use an a-value of 0.035±0.003 (Lai et al., 2008) and an alpha attenuation factor of 0.40±0.05, consistent with Martin et al. (2014).

For radionuclide concentration measurements, the sediment from the outer part of the tubes was dried at 110 °C for 24 hours, ground, mixed with wax, and cast into cup- or disc-shaped moulds. After a minimum of three weeks of storage, radionuclide concentrations were measured using high-resolution gamma spectrometry (Murray et al., 1987, 2018) and converted into infinite matrix dry dose rates using the conversion factors of Cresswell et al. (2018). The cosmic ray contribution was calculated based on Prescott and Hutton (1994).

To obtain reliable in situ water contents for the Holocene part of the section we dug two pits (2 m by 1 m) on top of the plateau, ~35 m from the edge of the cliff where our KH-II section was dug. One pit was dug after the summer (dry) season in October 2002 and the second one after the winter (wet) season in May 2023. In each pit, seven samples were collected during digging the pit until a depth ~2 m. Samples were double-packed in plastic zip bags water contents (weight water/dry weight x 100, %) measured upon arrival in the laboratory in Denmark (Table S3). For samples 228848 to H28815, water content measurements were done on the inside material that was most wet when opening the tubes.

4. Results

4.1. Stratigraphy of the upper part of the Khonako II section

Unit 1 (0.0 to 2.0 m) can be divided into two layers: the Holocene soil (layer 1) and a weakly reworked loess (layer 2). Layer 1 (0.0–0.8 m) is subdivided into four horizons: A (0-0.3 m): Light loam dark, gray, dry, highly porous, organic rich; B (0.3-0.5 m): Medium loam, dark gray, dense, porous, blocky-prismatic structure; Bm (0.5-0.6 m): Medium loam, brown, porous, prismatic structure, krotovinas with light sediments from lower layers; BCcaz (0.6-0.8 m): Medium loam, light beige, dense, highly porous, blocky, considerable $CaCO_3$, krotovinas with dark material from upper soil. Layer 2 (0.8-2.0 m) is loam, light beige, dry, dense, coarse-medium-highly porous, blocky, with considerable $CaCO_3$ and containing krotovinas with material from the upper soil. Unit 2 (2.0 to 12.25 m) corresponds to most of loess unit L1

and is divided into two layers (layers 3 and 4). Layer 3 (2.0-10.2 m) is loam, light beige, porous, massive, homogeneous, with rare carbonate veins. It is typical loess. Layer 4 (10.20-12.25 m) is loam yellow and brown with rare bioliths, $CaCO_3$ in small pores, and carbonate nodules up to 5 cm in diameter. It is identified as an interstadial palaeosol.

Fig. 2.

4.2. Dose rates

The total dose rates are presented in Table S1, and the radioelement concentrations, dry alpha, dry beta, and dry gamma dose rates in Table S2. The dose rate values are typical for loess, with an average of 3.50±0.07 Gy ka^{-1} (n=37) for quartz. A clear trend can be seen with the highest dose rate values for the four samples in the upper part of the Holocene soil and a decrease towards the L1 unit. Quartz dose rates range from 3.0±0.2 (sample 228849) to 4.7±0.2 (sample 228842) Gy ka^{-1} in the Holocene soil, and feldspar dose rates range from 3.5±0.2 to 5.3±0.3 Gy ka^{-1}. The L1 dose rates are homogenous with average values of 3.38±0.02 Gy ka^{-1} (n = 30) for quartz and 3.96±0.03 Gy ka^{-1} for feldspar. The ^{210}Pb to ^{226}Ra ratio of 0.98±0.03 (n=20) indicates no radon loss over the last few decades (De Corte et al., 2006). Individual ^{238}U analyses are insufficiently precise to allow us to discuss the degree of possible disequilibrium in individual samples. However, the unweighted average ^{226}Ra to ^{238}U ratio is 1.30±0.05 (n=30), omitting ratios with an uncertainty of >50%. We conclude that, on average, there may be evidence for a weak disequilibrium in the first part of the ^{238}U decay series.

The average water content of the samples collected from the pit after the dry season is 9±1% and increases to 17±2% after the wet season. To best account for the seasonal variability, an average value of 13±5% was chosen for the wet dose rate calculations of the upper Holocene part of the section (samples 228842 to 228847, see also discussion below).

For samples 228848 to H28815 (L1 unit), the average measured water content is 20±2%, but sample 228860 gave a maximum value of 29%. We consider this value to be the most representative of the present water content, as we suspect a dry out from the trenches before sampling and from inside the tubes.

The long-term burial water content for the L1 samples was then calculating following equation:

$$\frac{duration_{Hol} * w.c._1 + (age_{sample} - duration_{Hol}) * w.c._2}{age_{sample}}$$

Where $w.c._1$ corresponds to the measured water content in the Holocene soil, and $w.c._2$ to the maximum observed water content value from layer 3. The Holocene duration ($duration_{Hol}$) is assumed to be 11 ka. Since a hiatus was identified between 1.3 and 1.4 metres depth (see discussion), we expanded the $duration_{Hol}$ to 13 ka for samples between 1.41 and 2.45 m depth to reflect the successive burial, exposure, and re-burial events of the sediment. Our model follows an iterative process, where the initial water content used in the calculation of the quartz OSL age (age_{sample}) is updated until convergence with the modelled water content. The resulting modelled water content values are displayed in Table S4, and an uncertainty of 5% was assumed.

4.3. Quartz OSL characteristics

The inset in Fig. 3a shows a typical quartz OSL stimulation curve (sample 288881). It is very similar in shape to that from a known fast-component dominated sample, also shown (Risø calibration quartz, Hansen et al., 2015). Fig. 3a shows a typical quartz dose response curve (DRC) from sample 228881. Also shown is a single exponential function (EXP, dashed line), which clearly does not fit the data well. However, an exponential function with a linear component (EXPLIN), where the linear component becomes dominant at ~100 Gy, fits the data adequately. The natural signal is then interpolated on the dose response curve up to ~120 Gy, and the EXPLIN fit was chosen for all the samples. For doses below 60 Gy, a single saturating exponential function fit of the dose response curve was also satisfactory. Fig. 3b shows that the estimated dose is independent of the chosen preheat temperature ranging between 200 and 300 °C. The cutheat temperature is 40 °C lower than the preheat temperature. Therefore, a preheat of 240 °C and a cut-heat of 200 °C were chosen for further measurements.

A series of dose recovery tests (Murray, 1996) was performed for samples 228842, 228844, 228855, and 228870, using 24 aliquots per sample except for sample 228842 (n=36), with given doses close to the estimated natural doses. The samples were bleached twice using the blue LEDs at room temperature for 100 s (with an intervening pause of 10 ks) to remove the natural signal prior to giving a beta dose ranging between 12 and 76 Gy, followed by measurement. The resulting ratios are shown in Fig. S1. The average dose recovery ratio is 1.06±0.01 (n=99), and we conclude that our SAR protocol is well-suited to determine a dose given to the sample before any heat treatment.

The arithmetic average D_e (Guérin et al., 2017) estimates are presented in Table S1 with the corresponding quartz ages.

Fig. 3.

4.4. Polymineral $pIRIR_{200,290}$ characteristics

The $pIRIR_{290}$ dose response curve is well-represented by a single saturating exponential function (Fig. 4a). The estimated D_e seems to be independent of the first IR stimulation temperature for first IR temperature above 50°C (Fig. 4b). The first IR stimulation temperature was chosen to be 200°C to ensure the stability of the signal even at high doses (Li and Li, 2012b; Stevens et al., 2018). A sample from the Holocene soil and one from the L1 unit (228842 and 228871) were bleached in a solar simulator (Hönle SOL2 at a distance of 80 cm) for eight days for a dose recovery test. First, residuals of 9±2 Gy (n=5, 228842) and 23±1 Gy (n=5, 228871) were measured. Secondly, 36 solar-bleached aliquots were given beta doses of 27 Gy (228842) or 115 Gy (228871). These doses were then measured using test doses (TDs) of 30%, 50%, and 100% of the given dose (six aliquots per treatment). For a given dose of 27 Gy, the average dose recovery ratios (after subtraction of the measured residual dose) are 1.07±0.10 (TD 30%), 1.20±0.13 (TD 50%), and 1.23±0.10 (TD 100%), and the corresponding ratios for a given dose of 115 Gy are 1.17±0.05, 1.18±0.04 and 1.01±0.02 (Fig 4c.), respectively. The dose recovery ratios in the low dose experiment are all consistent with each other, but it should be noted that the ratios are poorly known because of the large uncertainty associated with the residual measurements. In the high dose experiment, the dose recovery ratio is only acceptable when the test dose is equal to the given dose.

A dose recovery test was undertaken using a single-aliquot regeneration and added dose (SARA) protocol (Mejdahl and Bøtter-Jensen, 1994) on sample 228842 (youngest sample with a polymineral dose of 29.3±3.4 Gy) to investigate further the influence of the test dose size. Doses in the range of interest (40, 80, 160 Gy) were added to the natural dose. One set of 12 aliquots was measured with a TD of ~30% of the expected dose, and a second set of 12 aliquots was measured with a TD of 80-100% of the expected dose. In Fig. 4d, the measured doses are fitted with a linear function, from which the slope estimates the dose recovery ratio. Both a TD of ~30% and a TD of 80-100% give satisfactory results (slopes of 1.057±0.006 and 0.932±0.013, respectively).

In the SOL2 experiment, the dose recovery ratio is only acceptable when the test dose is equal to the given dose for a dose >100 Gy, but our SARA dose recovery experiment does not indicate a clear dependence of the dose recovery on the test dose size. Therefore, we conclude that our $pIRIR_{200,290}$ protocol seems to adequately correct for sensitivity change in a 30-100% TD range. All the Khonako II D_e measurements were made using a TD of ~100% of the estimated dose for consistency.

Fig. 4.

4.5. Quartz OSL and $pIRIR_{200,290}$ age comparison

It is known that pIRIR signals bleach significantly more slowly compared to quartz and usually include a hard-to-bleach component, which can lead to a significant dose overestimation for young samples (e.g., Buylaert et al., 2011, 2012; Zhang et al., 2023). One way to assess how well the pIRIR signal was reset at deposition is to compare the quartz OSL ages and the pIRIR ages, assuming that in loess the quartz was well-bleached at burial (e.g., Murray et al., 2012; Stevens et al., 2018; Kurbanov et al., 2022; Taratunina et al., 2022; Volvakh et al., 2022). In this study, we examine the size of this residual by comparing the quartz OSL and $pIRIR_{200,290}$ ages and by measuring quartz OSL and $pIRIR_{200,290}$ polymineral D_e values on three modern dust samples (229101,03,04). The quartz OSL D_e values for these samples show they are modern (D_e < 0.5 Gy, Table S5). We used the average quartz and feldspar dose rates from our Khonako II data set to derive apparent ages for the modern dust, and plotted these $pIRIR_{200,290}$ and quartz ages with our Khonako II dataset (Fig. 5). Three samples from Khonako II (228846,-47,-48) were not taken into account in the comparison; they display an unusual high age discrepancy of ~ 7-5 ka and are located in layer 2, where evidence of bioturbation and reworking processes have been detected (see discussion).

The data are well-represented by a linear fit (of slope unity). The intercept is 2.25±0.09 ka on the $pIRIR_{200,290}$ age axis. From this intercept and the average feldspar dose rate in Khonako II, we deduce that the residual offset is 9.2±0.4 Gy. This value has been subtracted from all our $pIRIR_{200,290}$ doses. It is interesting to note that our residual $pIRIR_{200,290}$ offset is very similar to other measured offsets in loess, i.e., 5± 2 Gy (Stevens et al., 2018) and 8±3 Gy (Taratunina et al., 2022) as well as the $pIRIR_{50,290}$ 10±2 Gy measured on polymineral fine-grains from modern/young Chinese dust samples (Buylaert et al., 2011). Table S1 summarises the quartz OSL and $pIRIR_{200,290}$ ages (with and without residual dose subtraction). 80% of our $pIRIR_{200,290}$ ages are statistically consistent (at 95% confidence, random uncertainties only) with the quartz OSL ages (Table S1, Figure 2). Omitting the three samples mentioned above (228846,-47,-48), 87% are consistent with each other (96% if total uncertainties are used).

Fig. 5.

4.6. Age-depth modelling

A Bayesian model was run using the Bacon software (Blaauw and Christen, 2011) on the 30 quartz OSL and $pIRIR_{200,290}$ ages, using only the random component of the age uncertainty. The following settings were used to run the model: a prior accumulation rate of 50 cm ka^{-1}

(acc.mean=(50)) and thick = 10. Ages estimates were produced every 5 cm. Fig. 2 compares magnetic susceptibility (Fig. 2b), the luminescence ages with the Bayesian model (at 95% confidence) (Fig. 2c), and the dust accumulation rates calculated from the median Bayesian age estimates (Fig. 2d).

5. Discussion

Chapot et al. (2012) and Timar-Gabor and Wintle (2013) showed that the quartz laboratory dose response curve for Chinese and Romanian loess is best described using a sum of two saturating exponential functions while the natural signal follows a single saturating exponential function, which saturates significantly faster than the laboratory curve. The divergence between the two curves occurs at 100-150 Gy. The laboratory dose response curves for quartz OSL from Tajik loess also display non-single exponential growth above ~100 Gy. The largest measured quartz dose in this study is ~120 Gy and because of the good agreement between quartz OSL ages and $pIRIR_{200,290}$ feldspar ages, we deem our overall quartz chronology reliable over this age range. However, there is a need for more studies with independent age control and reliable natural dose response curves to fully examine the reliability of quartz OSL in the high dose range, where laboratory dose response curves are not well-represented by a single saturating exponential function.

According to the Bayesian chronological model of the Khonako II section, the upper part of L1 (2.0-7.9 m in unit 2) was deposited between ~39 and ~21 ka, during the end of MIS 3 and first part of MIS 2. However, the Bayesian approach shows methodological limits for the age estimate of layer 2 (0.8-2 m). Based on the individual luminescence ages, we identified a hiatus between 1.41 and 1.31 m in layer 2. Its duration varies depending on whether the quartz OSL chronology or the polymineral $pIRIR_{200,290}$ chronology is examined. When considering the individual $pIRIR_{200,290}$ ages, the hiatus would be between ~19 ka and 10 ka, and between ~15 and 7 ka when looking at the individual quartz OSL ages. The Bayesian model gives a shorter estimate of the hiatus duration (3 ka, compared to 9 and 7 ka). This can be explained by the mathematical construction of the model regarding the changes in accumulation rates.

The Bacon model (Blaauw and Christen, 2011) is an iterative model that includes a memory factor, w : the accumulation rate at a given depth is a weighted average of the accumulation rate of the previous depth and an independent noise, with prior density functions for both the memory factor and the independent noise. In their paper, Blaauw and Christen (2011) point to the resulting issue regarding hiatuses and any other sharp variation in the accumulation rate; their model is not adapted to such discontinuities in the accumulation rate. Therefore, they

recommend that any profile is cut into segments and the model run on each part separately; this segmentation should be based on external information (e.g., sedimentological characteristics). However, since it is the purpose of our geochronological study to identify such discontinuities, we are unable to define the different accumulation regimes before age measurements. As a consequence, we expect that Bacon will not describe discontinuities satisfactorily simply because it is, by its nature, not adapted to such features.

The Bayesian model is, therefore, not suitable to describe the sharp changes in sedimentation rates occurring in layer 2. Nonetheless, we consider the Bayesian chronology reliable for the samples of the upper part of unit 1, which show no inversion or significant discrepancy between the quartz OSL and the $pIRIR_{200,290}$ ages (0-1 m); the sedimentation then appears to have been continuous during ~8 and ~3 ka.

The hiatus was not identified in the field, but the rapid increase of the magnetic susceptibility at this depth confirms that it occurred at the transition period between the Holocene and the LGM (Constantin et al, 2019). Therefore, the LGM-Holocene boundary does not correspond to the bottom of Unit 1 (2 m). We propose the following model to explain the hiatus formation and the discrepancy between the quartz and polymineral ages: (1) At the end of the LGM, dust continued to accumulate until the Late Glacial time (~12 ka). Then, (2) an erosion event possibly linked to climate change deflated the surface until sediments which were deposited between 17-18 ka were exposed. (3) Soil processes reworked the exposed erosional boundary (layer 2, unit 1), and the resulting short sunlight re-exposure of the surface led to heterogeneous bleaching of the quartz grains before (4) reburial by continuing deposition. Because feldspar signals bleach more slowly, they were re-buried before losing much of their signal. But, animals and soil processes could potentially also have moved some modern material to the top of L1, and our samples could have been taken inadvertently from the many krotovinas identified in layer 2.

Dust accumulation rates (DAR) have been calculated and plotted as a function of age in Figure 2d. The end of MIS 3 is characterised by a change in the DAR at ~ 36.5 ka, with an increase from ~23 to 33 cm ka^{-1}. The average DAR during MIS 2 is ~ 41 cm ka^{-1}, but a peak in the accumulation reaches 71 cm ka^{-1} at ~ 21 ka. It is interesting to note that this high accumulation rate leads to indistinguishable luminescence ages between 20 and 23 ka. The DAR decreases after the LGM, to ~16 cm ka^{-1} during the Holocene.

Similar observations have been reported for other Tajik loess deposits. At the Hoalin section in Southern Tajikistan, Wang et al. (2018) obtained DARs ranging from 46 cm ka^{-1} to 54 cm ka^{-1} for the MIS 2 deposit. The DARs then decrease to ~2-5 cm ka^{-1} between 21 and 14 ka.

Yang et al. (2020) also reported a sharp decrease in dust accumulation between the LGM and the Holocene at a section located 10 km east of Dushanbe, with DARs ranging from ~56.8 to 6.0 cm ka^{-1}. Luminescence dating of Holocene soils in various parts of Tajikistan also show several erosion events both during LGM and in the Holocene (Murray et al., to be submitted). At the Darai Kalon section, the Holocene deposit is missing (Frechen and Dodonov, 1998) and the new luminescence chronology at the Kuldara section (Buylaert et al., this issue) shows that the upper stratigraphic unit is a reworked MIS 3 loess, it did not accumulate during the Holocene. Discontinuities in the sedimentary record have also been identified in other loess deposits across Arid Central Asia (Frechen et al., 2009; Lauer et al. 2017, Song et al., 2021, Zhang et al., 2020).

Our study shows no evidence of pedogenesis at the end of MIS 3 and during MIS 2 in the Khonako II section, which, together with the DARs and the firm magnetic susceptibility properties of loess, argues for stable dry and cold conditions in the piedmonts of the Pamir Mountains (Meshcheryakova et al., 2023). Even though our data provide additional evidence for a deflation event or soil reworking processes between the LGM and the Holocene, the Khovaling plateau was still dominated by active loess sedimentation over the last ~39 ka.

6. Conclusion

We have applied high-resolution quartz OSL and $pIRIR_{200,290}$ dating to the upper part of the Khonako II section. The elevated temperature polymineral pIRIR signal has satisfactory luminescence characteristics, and the quartz OSL ages are generally consistent with the pIRIR ages. This indicates that our quartz doses can be reliably determined up to ~120 Gy, despite the addition of a linear component to the dose response curve fit. The calculated residual of the pIRIR signal is equivalent to 9.2±0.4 Gy, which corresponds to a few ka, and thus is not significant when dating older samples.

The luminescence chronology confirms the deposition of the upper part of the Late Pleistocene loess unit during MIS 3 and 2, between ~20 and ~39 ka. Our results show an active and continuous sedimentation during the last part of the last glacial stage. The DAR increased at the end of MIS 3 and reached a peak during the LGM. The DAR is much lower during the Holocene. We also identified a hiatus at the transition between the LGM and the Holocene, which was not detected in the field. This highlights the importance of high-resolution dating in loess for reliable interpretation of climate proxies and accurate calculation of DAR.

Acknowledgments

This work was partly supported by NordForsk through the funding to "The timing and ecology of the human occupation of Central Asia", project number 105204. Yunus Baykal is thanked for help with preparation of gamma spectrometry samples.

Figure captions

Figure 1. Location of the Khonako II section (A-B) and general view of the upper part of the Khonako II section (C). The red band (C) indicates the studied sections. ©Ramona Schneider (A) and ©Gábor Újvári (B).

Figure 2. A. Stratigraphic chart of the upper part of the Khonako II section. The ages quoted on the stratigraphic chart are the measured OSL ages (in blue) and the $pIRIR_{200,290}$ ages (in red) after subtraction of a residual of 9.2±0.4 Gy. B. Frequency-dependent magnetic susceptibility. C. Luminescence ages and Bayesian chronological model. The quartz ages (blue circles) have been obtained by interpolation onto dose response curves fitted with a single exponential with a linear component function. The $pIRIR_{200,290}$ ages (red open circles) are given after subtraction of the residual. Bayesian modelling results (solid line) obtained using the Bacon Model (Blaauw and Christen, 2011) of the quartz OSL ages (without systematic uncertainties) are shown at 95% confidence (dashed lines). D. Dust accumulation rate (DAR) as a function of the Bayesian mean age estimates calculated every 5 cm.

Figure 3. Quartz luminescence characteristics. A) Typical dose response curve fitted with a single saturating exponential function (dashed line) and a single exponential with a linear component function (solid line). The inset shows the initial 5 s of a typical normalised OSL stimulation curve (sample 228881, note the initial 10 dead channels) as well as the corresponding curve for Risø calibration quartz (Hansen et al., 2015). B) Estimated average dose for sample 228844 as a function of preheat temperature. Each point is an average of 4 aliquots. The solid horizontal line indicates the average dose irrespective of preheat temperature and the dashed lines indicate the 68% confidence level. The solid vertical line indicates the chosen preheat temperature for measurement of all quartz samples.

Figure 4. Polymineral pIRIR characteristics. A) Typical polymineral $pIRIR_{200,290}$ dose response curve. B) Estimated average pIRIR(x,290) dose for sample 228845 as a function of the first IR stimulation temperature (x). Each point is an average of 6 aliquots, except for the 200 °C point (n=12). C) Dose recovery ratios for samples 228842 and 228871 bleached for 8 days in a solar simulator. D) Additive dose recovery experiment (SARA) on sample 228842 using test doses of 30% and 80-100% of the expected dose.

Figure 5. Comparison of the quartz OSL ages and the polymineral $pIRIR_{200,290}$ ages (solid circles). The black dashed line corresponds to the $y=x$ line; the solid black line is a linear fit with a forced unit slope of the data and an intercept of 2.18±0.09 ka. The blue squares represent the modern dust samples. The samples (228846,-47,-48) in the ellipse are not considered in the fitting (see text for details).

Supplementary information

Figure S1. Quartz dose recovery ratios for samples 228842, 228844, 228855, and 228870 for an EXPLIN fit of the quartz dose response curve.

Table S1. Quartz and polymineral luminescence results. w.c. - water content, (n_a) - number of accepted aliquots. Uncertainties are given at 1 σ and contain both random and systematic components. Samples with poor OSL IR depletion ratios are denoted with N.A. (no D_e given).

Table S2. Radionuclide concentrations, dry alpha, beta and gamma dose rates.

Table S3. Water content values from the pits dug during autumn 2022 and spring 2023 seasons at the top of the plateau, ~35 m from the cliff where the Khonako II section is located.

Table S4. Long-term burial water content model. The observed water content values and the Holocene duration are used as input in the model. Note: for samples 228842 to 228847, the average of the observed water content values from the pits (13±5%) was used for the dose rate calculation.

Table S5. Modern dust sample results: quartz OSL, IR_{50}, $pIRIR_{50,180}$, $pIRIR_{200,290}$ D_e values. IR50 results come from the $pIRIR_{50,180}$ protocol. IQR (interquartile range) criterion was used to reject outliers (±1.5xIQR), number of outliers denoted with (nr).

Bibliography

Autzen, M., Andersen, C.E., Bailey, M., Murray, A.S., 2022. Calibration quartz: An update on dose calculations for luminescence dating. Radiation Measurements 157, 106828. https://doi.org/10.1016/j.radmeas.2022.106828

Ballarini, M., Wallinga, J., Wintle, A.G., Bos, A.J.J., 2007. A modified SAR protocol for optical dating of individual grains from young quartz samples. Radiation Measurements 42, 360–369. https://doi.org/10.1016/j.radmeas.2006.12.016

Blaauw, M., Christen, J.A., 2011. Flexible palaeoclimate age-depth models using an autoregressive gamma process. Bayesian Analysis 6, 457–474. https://doi.org/10.1214/11-BA618

Bøtter-Jensen, L., Thomsen, K.J., Jain, M., 2010. Review of optically stimulated luminescence (OSL) instrumental developments for retrospective dosimetry. Radiation Measurements 45, 253–257. https://doi.org/10.1016/j.radmeas.2009.11.030

Buylaert J.-P., Challier A., Taratunina1 N.A., Kulakova E.P., Thomsen K.J., Utkina A.O., P.M., Tokareva O.A., Anoikin A.A., Khujageldiev T.U., Karayev A.C., Ubaydulloev N.K., Murray A.S., Kurbanov R.N. A luminescence dating study of the upper part of the loess-palaeosol sequence at Kuldara, Khovaling Loess Plateau, Tajikistan. Submitted to Quaternary Geochronology.

Buylaert, J.P., Murray, A.S., Vandenberghe, D., Vriend, M., De Corte, F., Van den haute, P., 2008. Optical dating of Chinese loess using sand-sized quartz: Establishing a time frame for Late Pleistocene climate changes in the western part of the Chinese Loess Plateau. Quaternary Geochronology 3, 99–113. https://doi.org/10.1016/j.quageo.2007.05.003

Buylaert, J.P., Vandenberghe, D., Murray, A.S., Huot, S., De Corte, F., Van den Haute, P., 2007. Luminescence dating of old (>70ka) Chinese loess: A comparison of single-aliquot OSL and IRSL techniques. Quaternary Geochronology 2, 9–14. https://doi.org/10.1016/j.quageo.2006.05.028

Buylaert, J.-P., Thiel, C., Murray, A., Vandenberghe, D., Yi, S., Lu, H., 2011. IRSL and post-IR IRSL residual doses recorded in modern dust samples from the Chinese Loess Plateau. Geochronometria 38, 432–440. https://doi.org/10.2478/s13386-011-0047-0

Buylaert, J.-P., Thiel, C., Murray, A.S., Jain, M., Thomsen, K.J., Sohbati, R., 2012. Extending the luminescence dating age range using feldspar, Quaternary Geochronology 17, 55-67.

Buylaert, J.-P., Yeo, E.-Y., Thiel, C., Yi, S., Stevens, T., Thompson, W., Frechen, M., Murray, A., Lu, H., 2015. A detailed post-IR IRSL chronology for the last interglacial soil at the Jingbian loess site (northern China). Quaternary Geochronology 30, 194–199. https://doi.org/10.1016/j.quageo.2015.02.022

Chapot, M.S., Roberts, H.M., Duller, G.A.T., Lai, Z.P., 2012. A comparison of natural- and laboratory-generated dose response curves for quartz optically stimulated luminescence signals from Chinese Loess. Radiation Measurements 47, 1045–1052. https://doi.org/10.1016/j.radmeas.2012.09.001

Constantin, D., Veres, D., Panaiotu, C., Anechitei-Deacu, V., Groza, S.M., Begy, R., Kelemen, S., Buylaert, J.P., Hambach, U., Marković, S.B. and Gerasimenko, N., 2019.

564 Luminescence age constraints on the Pleistocene-Holocene transition recorded in loess
565 sequences across SE Europe. Quaternary Geochronology, 49, 71-77.

566 Cresswell, A.J., Carter, J., Sanderson, D.C.W., 2018. Dose rate conversion parameters:
567 Assessment of nuclear data. Radiation Measurements 120, 195–201.
568 https://doi.org/10.1016/j.radmeas.2018.02.007

569 Cunningham, A.C., Wallinga, J., 2010. Selection of integration time intervals for quartz OSL
570 decay curves. Quaternary Geochronology 5, 657–666.
571 https://doi.org/10.1016/j.quageo.2010.08.004

572 Dave, A.K., Timar-Gabor, A., Scardia, G., Safaraliev, N., Fitzsimmons, K.E., 2022. Variation
573 in Luminescence Characteristics and Paramagnetic Defect Centres in Fine-Grained Quartz
574 From a Loess-Palaeosol Sequence in Tajikistan: Implications for Provenance Studies in
575 Aeolian Environments. Frontiers in Earth Science 10, 835281.
576 https://doi.org/10.3389/feart.2022.835281

577 De Corte, F., Vandenberghe, D., De Wispelaere, A., Buylaert, J.-P., Van den Haute, P., 2006.
578 Radon loss from encapsulated sediments in Ge gamma-ray spectrometry for the annual
579 radiation dose determination in luminescence dating. Czech J Phys 56, D183–D194.
580 https://doi.org/10.1007/s10582-006-1016-3

581 Ding, Z.L., Ranov, V., Yang, S.L., Finaev, A., Han, J.M., Wang, G.A., 2002. The loess record
582 in southern Tajikistan and correlation with Chinese loess. Earth and Planetary Science Letters
583 200, 387–400. https://doi.org/10.1016/S0012-821X(02)00637-4

584 Dodonov, A.E., 1991. Loess of Central Asia. GeoJournal 24, 185–194.
585 https://doi.org/10.1007/BF00186015

586 Dodonov, A.E., 2002. Quaternary Period of Central Asia: Stratigraphy, Correlation,
587 Palaeogeography. GEOS, Moscow. (In Russian)

588 Dodonov, A.E., Baiguzina, L.L., 1995. Loess stratigraphy of Central Asia: Palaeoclimatic and
589 palaeoenvironmental aspects. Quaternary Science Reviews 14, 707–720.
590 https://doi.org/10.1016/0277-3791(95)00054-2

591 Dodonov, A.E., Sadchikova, T.A., Sedov, S.N., Simakova, A.N., Zhou, L.P., 2006.
592 Multidisciplinary approach for palaeoenvironmental reconstruction in loess-palaeosol studies
593 of the Darai Kalon section, Southern Tajikistan. Quaternary International 152–153, 48–58.
594 https://doi.org/10.1016/j.quaint.2005.12.001

595 Dodonov, A.E., Zhou, L., 2008. Loess deposition in Asia: its initiation and development
596 before and during the Quaternary. Episodes Journal of International Geoscience 31, 222–225.
597 https://doi.org/10.18814/epiiugs/2008/v31i2/006

598 Duller, G.A.T., 2003. Distinguishing quartz and feldspar in single grain luminescence
599 measurements. Radiation Measurements 37, 161–165. https://doi.org/10.1016/S1350-
600 4487(02)00170-1

601 Frechen, M., Dodonov, A.E., 1998. Loess chronology of the Middle and Upper Pleistocene in
602 Tadjikistan. Geol Rundsch 87, 2–20. https://doi.org/10.1007/s005310050185

Frechen, M., Kehl, M., Rolf, C., Sarvati, R., Skowronek, A., 2009. Loess chronology of the Caspian Lowland in Northern Iran. Quaternary International 198, 220–233. https://doi.org/10.1016/j.quaint.2008.12.012

Guérin, G., Christophe, C., Philippe, A., Murray, A.S., Thomsen, K.J., Tribolo, C., Urbanova, P., Jain, M., Guibert, P., Mercier, N., Kreutzer, S., Lahaye, C., 2017. Absorbed dose, equivalent dose, measured dose rates, and implications for OSL age estimates: Introducing the Average Dose Model. Quaternary Geochronology 41, 163–173. https://doi.org/10.1016/j.quageo.2017.04.002

Hansen, V., Murray, A., Buylaert, J.-P., Yeo, E.-Y., Thomsen, K., 2015. A new irradiated quartz for beta source calibration. Radiation Measurements 81, 123–127. https://doi.org/10.1016/j.radmeas.2015.02.017

Hansen, V., Murray, A., Thomsen, K., Jain, M., Autzen, M., Buylaert, J.-P., 2018. Towards the origins of over-dispersion in beta source calibration. Radiation Measurements120, 157–162. https://doi.org/10.1016/j.radmeas.2018.05.014

Huntley, D.J., Baril, M.R., 1997. The K content of the K-feldspars being measured in optical dating or in thermoluminescence dating. Ancient Tl 15, 11–13.

Kurbanov, R.N., Buylaert, J.-P., Stevens, T., Taratunina, N.A., Belyaev, V.R., Makeev, A.O., Lebedeva, M.P., Rusakov, A.V., Solodovnikov, D., Költringer, C., Rogov, V.V., Streletskaya, I.D., Murray, A.S., Yanina, T.A., 2022. A detailed luminescence chronology of the Lower Volga loess-palaeosol sequence at Leninsk. Quaternary Geochronology 73, 101376. https://doi.org/10.1016/j.quageo.2022.101376

Lai, Z.P., Zöller, L., Fuchs, M., Brückner, H., 2008. Alpha efficiency determination for OSL of quartz extracted from Chinese loess. Radiation Measurements 43, 767–770. https://doi.org/10.1016/j.radmeas.2008.01.022

Lai, Z., 2010. Chronology and the upper dating limit for loess samples from Luochuan section in the Chinese Loess Plateau using quartz OSL SAR protocol. Journal of Asian Earth Sciences 37, 176–185. https://doi.org/10.1016/j.jseaes.2009.08.003

Lauer, T., Vlaminck, S., Frechen, M., Rolf, C., Kehl, M., Sharifi, J., Lehndorff, E., Khormali, F., 2017. The Agh Band loess-palaeosol sequence – A terrestrial archive for climatic shifts during the last and penultimate glacial–interglacial cycles in a semiarid region in northern Iran. Quaternary International 429, 13–30. https://doi.org/10.1016/j.quaint.2016.01.062

Li, B., Li, S.-H., 2012a. Luminescence dating of Chinese loess beyond 130 ka using the non-fading signal from K-feldspar. Quaternary Geochronology 10, 24–31. https://doi.org/10.1016/j.quageo.2011.12.005

Li, B., Li, S., 2012b. A reply to the comments by Thomsen et al. on "Luminescence dating of K-feldspar from sediments: a protocol without anomalous fading correction." Faculty of Science - Papers (Archive) 49–51. https://doi.org/10.1016/j.quageo.2011.10.001

Li, B., Li, S.-H., 2011. Luminescence dating of K-feldspar from sediments: A protocol without anomalous fading correction. Quaternary Geochronology 6, 468–479. https://doi.org/10.1016/j.quageo.2011.05.001

Li, Y., Zhou, L., 2021. Variations of Thermally and Optically Stimulated Luminescence Sensitivity of Loess and Pedocomplex Samples from Southern Tajikistan, Central Asia. Geochronometria 48, 242–252. https://doi.org/10.1515/geochr-2015-0118

Li, G., Wen, L., Xia, D., Duan, Y., Rao, Z., Madsen, D.B., Wei, H., Li, F., Jia, J., Chen, F., 2015. Quartz OSL and K-feldspar pIRIR dating of a loess/palaeosol sequence from arid central Asia, Tianshan Mountains, NW China. Quaternary Geochronology 28, 40–53. https://doi.org/10.1016/j.quageo.2015.03.011

Li, G., Yang, H., Stevens, T., Zhang, X., Zhang, H., Wei, H., Zheng, W., Li, L., Liu, X., Chen, J., Xia, D., Oldknow, C., Ye, W., Chen, F., 2020. Differential ice volume and orbital modulation of Quaternary moisture patterns between Central and East Asia. Earth and Planetary Science Letters 530, 115901. https://doi.org/10.1016/j.epsl.2019.115901

Martin, L., Mercier, N., Incerti, S., 2014. Geant4 simulations for sedimentary grains in infinite matrix conditions: The case of alpha dosimetry. Radiation Measurements 70, 39–47. https://doi.org/10.1016/j.radmeas.2014.09.003

Mejdahl, V., 1979. Thermoluminescence dating: beta-dose attenuation in quartz grains. Archaeometry 21, 61-72.

Mejdahl, V., Bøtter-Jensen, L., 1994. Luminescence dating of archaeological materials using a new technique based on single aliquot measurements. Quaternary Science Reviews 13, 551–554. https://doi.org/10.1016/0277-3791(94)90076-0

Meshcheryakova, O.A., Kurbanov, R.N., Pavlov, V.E., 2023. Reconstructions of paleowind directions in the Pleistocene: Evidence from the anisotropy of magnetic susceptibility of the loess–paleosol series of Tajikistan and the Azov region. Izvestiya. Physics of the Solid Earth 59, 704–716.

Murray A., Challier A., Buylaert J.-P., Schneider R., Khormali F., Navi S.V., Sosin P., Kurbanov R.N. Did the surface soils to be used for calibration of Central Asian climate proxies form under the current climate? Quaternary Geochronology. To be submitted

Murray, A., Arnold, L.J., Buylaert, J.-P., Guérin, G., Qin, J., Singhvi, A.K., Smedley, R., Thomsen, K.J., 2021. Optically stimulated luminescence dating using quartz. Nat Rev Methods Primers 1, 72. https://doi.org/10.1038/s43586-021-00068-5

Murray, A.S., 1996. Developments in optically transferred luminescence and photo-transferred thermoluminescence dating: application to a 2000-year sequence of flood deposits. Geochimica et Cosmochimica Acta 60, 565–576.

Murray, A.S., Helsted, L.M., Autzen, M., Jain, M., Buylaert, J.P., 2018. Measurement of natural radioactivity: Calibration and performance of a high-resolution gamma spectrometry facility. Radiation Measurements 120, 215–220. https://doi.org/10.1016/j.radmeas.2018.04.006

Murray, A.S., Marten, R., Johnston, A., Martin, P., 1987. Analysis for naturally occuring radionuclides at environmental concentrations by gamma spectrometry. Journal of Radioanalytical and Nuclear Chemistry Articles 115, 263–288. https://doi.org/10.1007/BF02037443

683 Murray, A.S., Thomsen, K.J., Masuda, N., Buylaert, J.P., Jain, M., 2012. Identifying well-
684 bleached quartz using the different bleaching rates of quartz and feldspar luminescence
685 signals. Radiation Measurements 47, 688–695. https://doi.org/10.1016/j.radmeas.2012.05.006

686 Murray, A.S., Wintle, A.G., 2003. The single aliquot regenerative dose protocol: potential for
687 improvements in reliability. Radiation Measurements 37, 377–381.
688 https://doi.org/10.1016/S1350-4487(03)00053-2

689 Murray, A.S., Wintle, A.G., 2000. Luminescence dating of quartz using an improved single-
690 aliquot regenerative-dose protocol. Radiation Measurements 32, 57–73.
691 https://doi.org/10.1016/S1350-4487(99)00253-X

692 Parviz, N., Shen, Z., Yunus, M., Zulqarnain, S., 2020. Loess deposits in southern Tajikistan
693 (Central Asia): Magnetic properties and palaeoclimate. Quaternary Geochronology 60,
694 101114. https://doi.org/10.1016/j.quageo.2020.101114

695 Prescott, J.R., Hutton, J.T., 1994. Cosmic ray contributions to dose rates for luminescence and
696 ESR dating: Large depths and long-term time variations. Radiation Measurements 23, 497–
697 500. https://doi.org/10.1016/1350-4487(94)90086-8

698 Schäfer, J., Ranov, V.A., Sosin, P.M., 1998. The "Cultural Evolution" of man and the
699 chronostratigraphical background of changing environments in the loess palaeosol sequences
700 of Obi-Mazar and Khonako (Tadjikistan). Anthropologie (1962-) 36, 121–135.

701 Schmidt, C., Bösken, J., Kolb, T., 2018. Is there a common alpha-efficiency in polymineral
702 samples measured by various infrared stimulated luminescence protocols? Geochronometria
703 45, 160–172. https://doi.org/10.1515/geochr-2015-0095

704 Sohbati, R., Kook, M., Pirtzel, L.P., Thomsen, K.J., 2021. Safelight for OSL dating
705 laboratories: a follow-up study, Ancient TL 39.

706 Song, Y., Li, Y., Cheng, L., Zong, X., Kang, S., Ghafarpour, A., Li, X., Sun, H., Fu, X.,
707 Dong, J., Mamadjanov, Y., Orozbaev, R., Shukurov, N., Gholami, H., Shukurov, S., Xie, M.,
708 2021. Spatio-temporal distribution of Quaternary loess across Central Asia. Palaeogeography,
709 Palaeoclimatology, Palaeoecology 567, 110279. https://doi.org/10.1016/j.palaeo.2021.110279

710 Spooner, N.A., 1994. The anomalous fading of infrared-stimulated luminescence from
711 feldspars. Radiation Measurements 23, 625–632. https://doi.org/10.1016/1350-
712 4487(94)90111-2

713 Stevens, T., Buylaert, J.-P., Thiel, C., Újvári, G., Yi, S., Murray, A.S., Frechen, M., Lu, H.,
714 2018. Ice-volume-forced erosion of the Chinese Loess Plateau global Quaternary stratotype
715 site. Nat Commun 9, 983. https://doi.org/10.1038/s41467-018-03329-2

716 Taratunina, N.A., Buylaert, J.-P., Kurbanov, R.N., Yanina, T.A., Makeev, A.O., Lebedeva,
717 M.P., Utkina, A.O., Murray, A.S., 2022. Late Quaternary evolution of lower reaches of the
718 Volga River (Raygorod section) based on luminescence dating. Quaternary Geochronology
719 72, 101369. https://doi.org/10.1016/j.quageo.2022.101369

720 Thiel, C., Buylaert, J.-P., Murray, A., Terhorst, B., Hofer, I., Tsukamoto, S., Frechen, M.,
721 2011. Luminescence dating of the Stratzing loess profile (Austria) – Testing the potential of

an elevated temperature post-IR IRSL protocol. Quaternary International 234, 23–31. https://doi.org/10.1016/j.quaint.2010.05.018

Thomsen, K.J., Murray, A.S., Jain, M., Bøtter-Jensen, L., 2008. Laboratory fading rates of various luminescence signals from feldspar-rich sediment extracts. Radiation Measurements 43, 1474–1486. https://doi.org/10.1016/j.radmeas.2008.06.002

Tian, S., Sun, J., Zhang, Z., Abdulov, S., Cao, M., Gadoev, M., Oimahmadov, I., 2021. Loess deposits in the Tajik Basin, Central Asia: chronology, provenance and palaeoclimatic implications since the Last Glacial. Boreas 50, 147–166. https://doi.org/10.1111/bor.12467

Timar-Gabor, A., Wintle, A.G., 2013. On natural and laboratory generated dose response curves for quartz of different grain sizes from Romanian loess. Quaternary Geochronology 18, 34–40. https://doi.org/10.1016/j.quageo.2013.08.001

Volvakh, N.E., Kurbanov, R.N., Zykina, V.S., Murray, A.S., Stevens, T., Költringer, C.A., Volvakh, A.O., Malikov, D.G., Taratunina, N.A., Buylaert, J.-P., 2022. First high-resolution luminescence dating of loess in Western Siberia. Quaternary Geochronology 73, 101377. https://doi.org/10.1016/j.quageo.2022.101377

Wang, L., Jia, J., Li, G., Li, Z., Wang, X., Chen, F., 2018. Fine-grained quartz OSL dating chronology of loess sequence from southern Tajikistan: Implications for climate change in arid central Asia during MIS 2. Journal of Asian Earth Sciences 155, 116–123. https://doi.org/10.1016/j.jseaes.2017.11.001

Yang, S., Li, D., Liu, N., Zan, J., Liu, W., Kang, J., Murodov, A., Fang, X., 2020. Quartz optically stimulated luminescence dating of loess in Tajikistan and its palaeoclimatic implications for arid Central Asia since the Lateglacial. Palaeogeography, Palaeoclimatology, Palaeoecology 556, 109881. https://doi.org/10.1016/j.palaeo.2020.109881

Yi, S., Buylaert, J.-P., Murray, A.S., Thiel, C., Zeng, L., Lu, H., 2015. High resolution OSL and post-IR IRSL dating of the last interglacial–glacial cycle at the Sanbahuo loess site (northeastern China). Quaternary Geochronology 30, 200–206. https://doi.org/10.1016/j.quageo.2015.02.013

Yi, S., Buylaert, J.-P., Murray, A.S., Lu, H., Thiel, C., Zeng, L., 2016. A detailed post-IR IRSL dating study of the Niuyangzigou loess site in northeastern China. Boreas 45, 644–657. https://doi.org/10.1111/bor.12185

Yi, S., Li, X., Han, Z., Lu, H., Liu, J., Wu, J., 2018. High resolution luminescence chronology for Xiashu Loess deposits of Southeastern China. Journal of Asian Earth Sciences 155, 188–197. https://doi.org/10.1016/j.jseaes.2017.11.027

Zan, J., Ning, W., Heller, F., Fang, X., Zhang, W., Kang, J., 2022. Intensified Northern Hemisphere Glaciation Facilitates Continuous Accumulation of Late Pliocene Loess on the Western Margin of the Pamir. Geophysical Research Letters 49, e2022GL099629. https://doi.org/10.1029/2022GL099629

Zhang, J., Tsukamoto, S., Long, H., 2023. Testing the potential of pulsed post-IR IRSL dating on Chinese loess deposits. Quaternary Geochronology 78, 101469. https://doi.org/10.1016/j.quageo.2023.101469

762 Zhang, J., Zhou, X., Long, H., 2020. Late Quaternary loess accumulation at the Rudak section
763 in Uzbekistan, central Asia: Chronology and palaeoclimate implications. Palaeogeography,
764 Palaeoclimatology, Palaeoecology 547, 109695. https://doi.org/10.1016/j.palaeo.2020.109

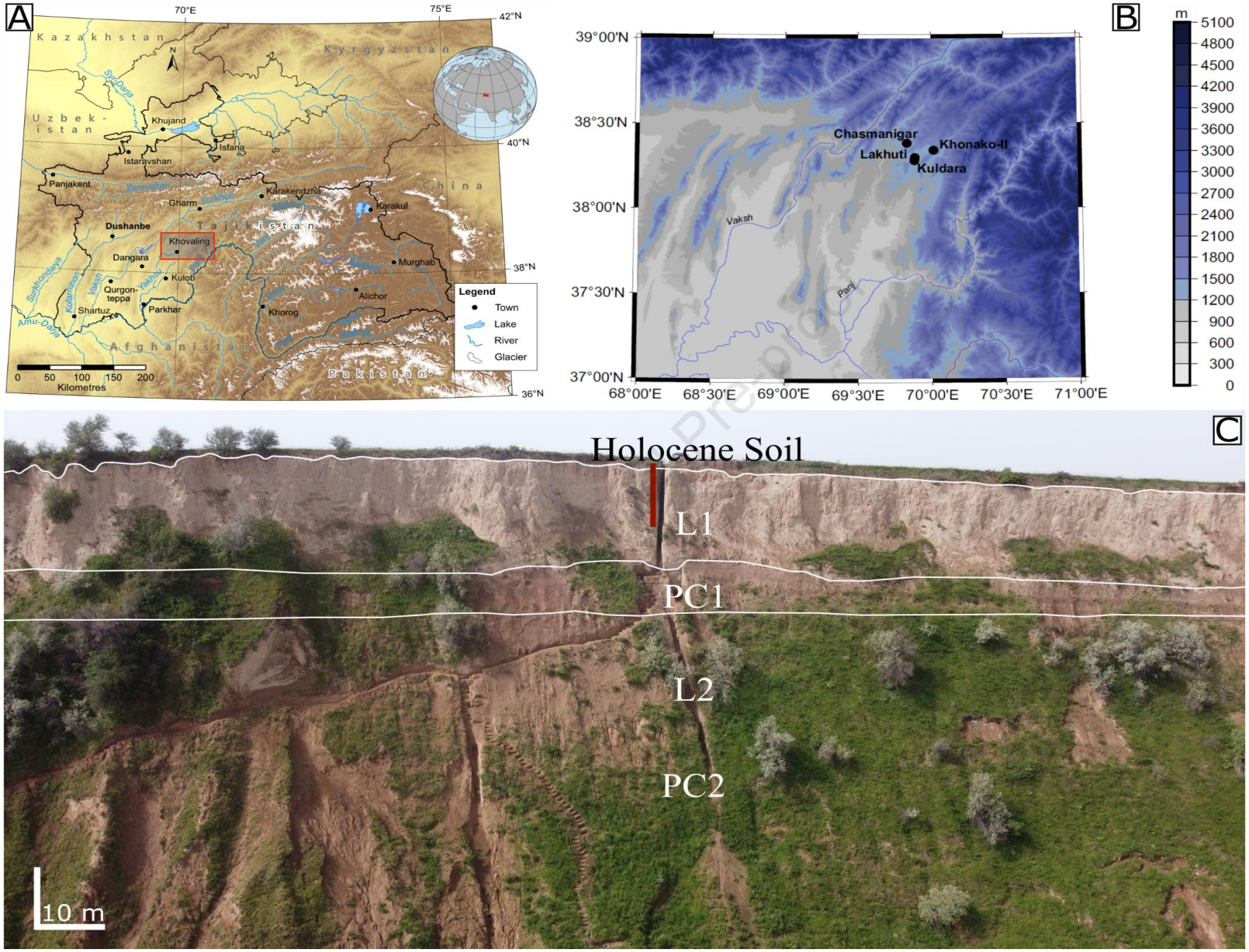

Figure 1

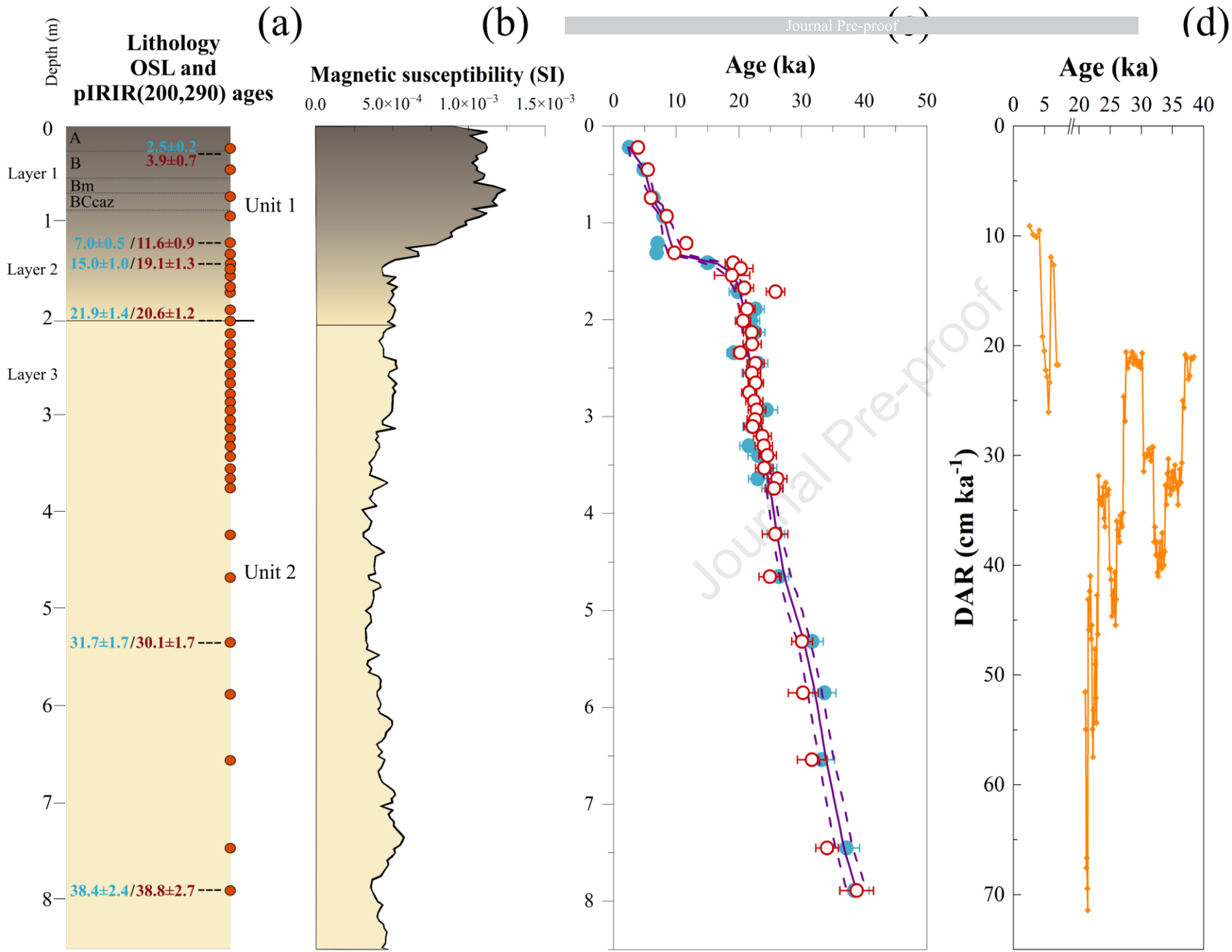

Figure 2

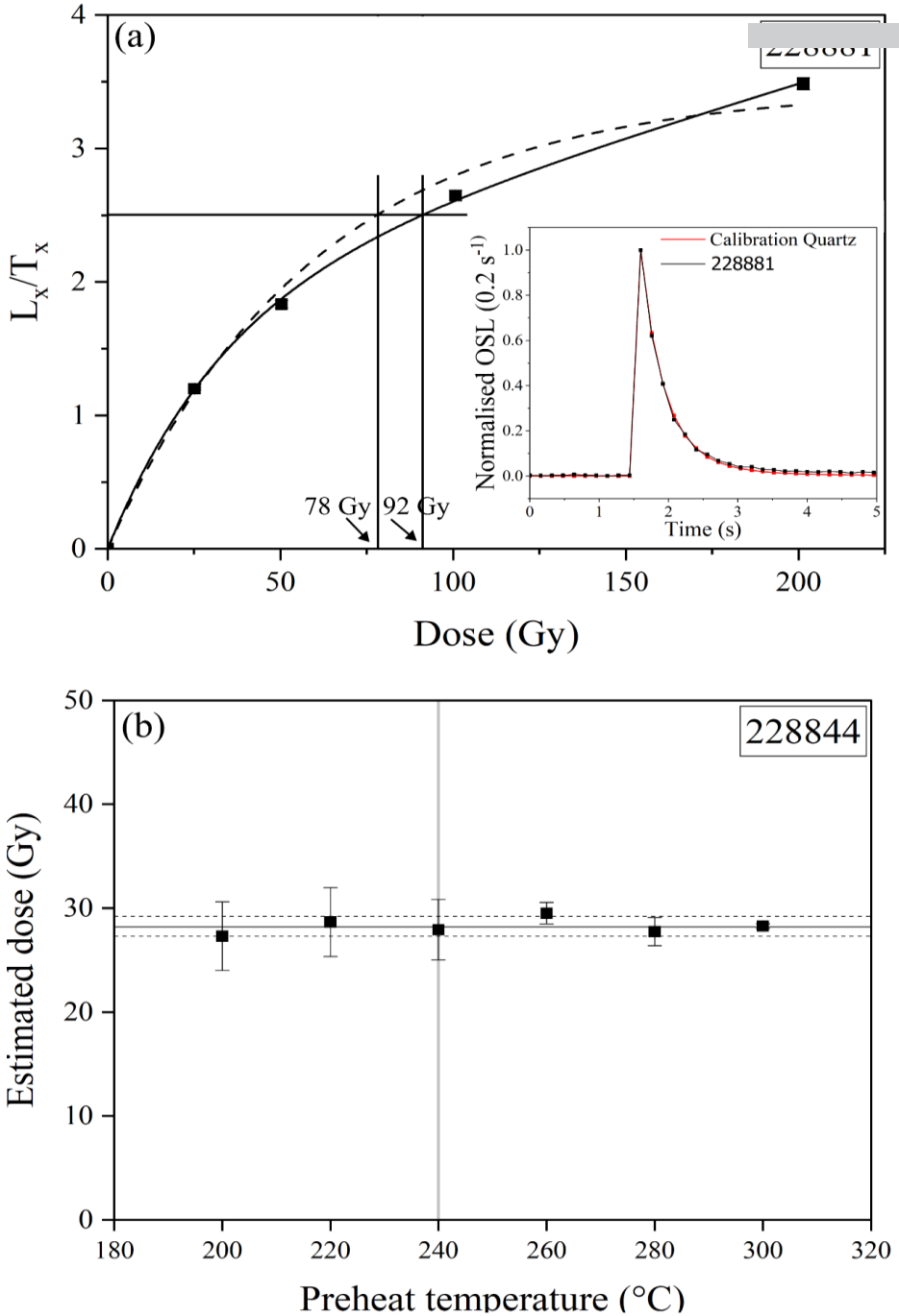

Figure 3

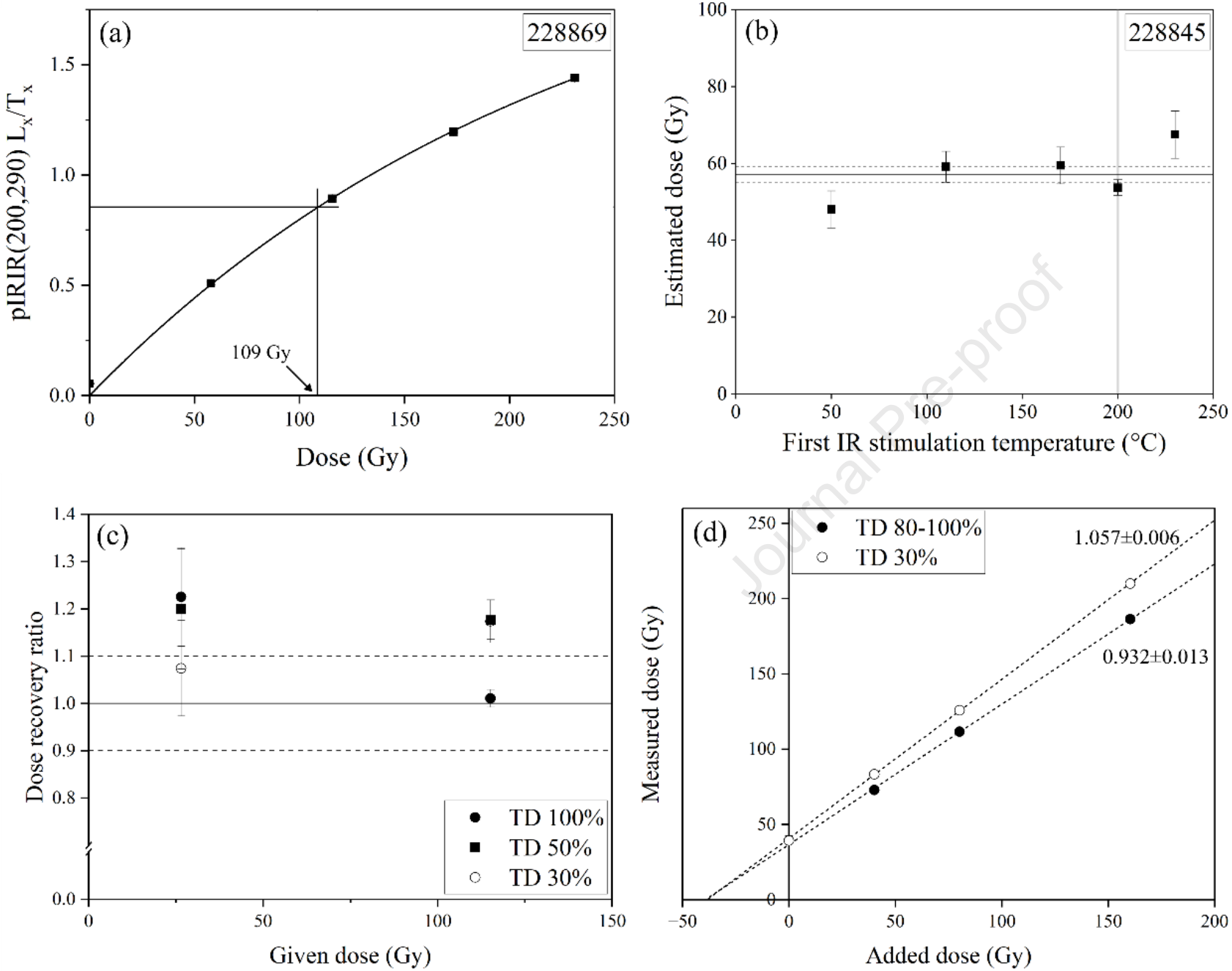

Figure 4

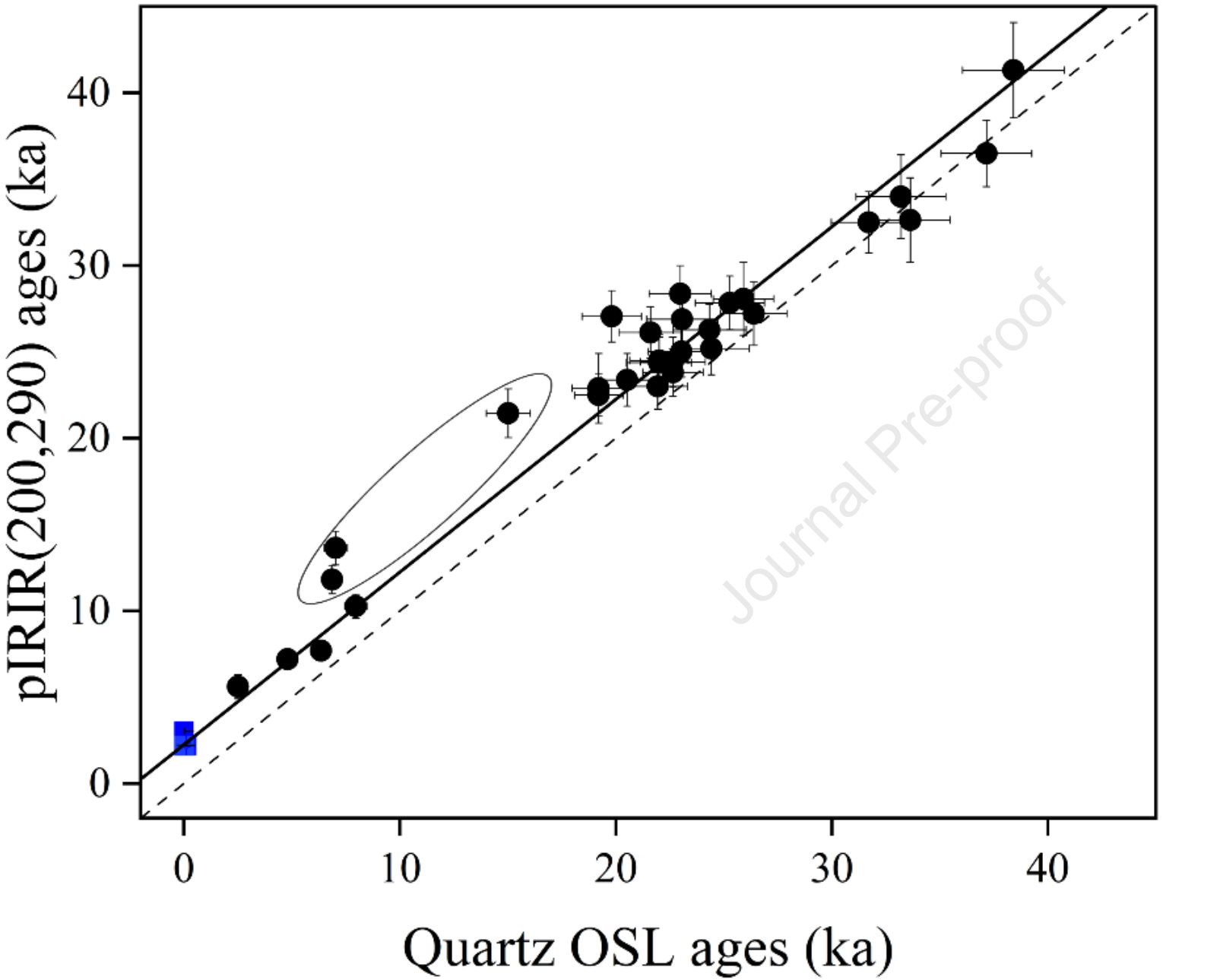

Figure 5

Declaration of interests

☐ The authors declare that they have no known competing financial interests or personal relationships that could have appeared to influence the work reported in this paper.

☒ The authors declare the following financial interests/personal relationships which may be considered as potential competing interests:

Jan-Pieter Buylaert reports financial support was provided by Nordic Council of Ministers. If there are other authors, they declare that they have no known competing financial interests or personal relationships that could have appeared to influence the work reported in this paper.